STRAIN MONITORING BY FIBER BRAGG GRATINGS IN THICK COMPOSITE CYLINDERS MANUFACTURING

M. Esposito[*], A. Martone[*], V. Antonucci[*], M. Zarrelli[*], M. Giordano[*]

[*] Institute for Polymers Composite and Biomaterials, National Research Council of Italy
Ple E Fermi, 1 80055 Portici (NA), Italy

Key words: FBG Strain Monitoring, Residual Stresses, Thick Composites Cylinders.

ABSTRACT

The autoclave process is the main and the most largely diffused technology for high quality polymer composite manufacturing. In autoclave, an heated and highly pressurized air flow allows the curing and the extremely effective compaction of the composite, achieving excellent mechanical properties of the composite. Nevertheless, the high exothermicity of the polymerization and the low thermal conductivity of the thermo-set matrix may increase the risk of the material failure during the manufacturing process. In this paper, the case of a thick composite cylinder that has shown some failures in the real manufacturing process is analysed. Fiber Bragg Gratings (FBG) optical sensors embedded in the composite cylinder during the manufacturing allowed the measurement of process induced strains for the validation of the numerical FEM model of the process, ad-hoc developed. The aim of the model is the evaluation of the risk of failure during cylinder manufacturing. The mechanical model takes into account geometry, stacking sequence, multistep manufacturing process, material thermo viscoelastic anisotropic behaviour and tool–composite interaction as well as heat transfer, cure kinetic and mechanical modelling of gelation during cure.

1 INTRODUCTION

Composite materials are widely used in several application where high mechanical performances of the material are crucial, such as the aerospace industry, thanks to their intrinsic benefits as low weight and high stiffness. Autoclave technology allows the achievement of excellent mechanical properties as well as the reduction of the stress concentration effect and the crack generation risk due to the porosity and dry spots. This is achieved through an extremely effective compaction of the composite, by the application of highly pressurized air flow inside the autoclave chamber.

However the strong exothermicity due to the crosslinking chemical polymerization reactions and the low material thermal conductivity may generate gradients of the chemical conversion and mechanical distortions due to inhomogeneous thermal expansion. For this reason, during the final cooling stage, significant stresses may build up inside component. In addition, the tool provides a further external constrain to the component free deformation during the processing, since its thermal expansion coefficients (CTE) is quite different than the composite one.

In the present work a structural model has been developed to predict the stress build-up and the risk of failure during the whole manufacturing cycle for a cylindrical composite laminate geometry. The model, based on Finite Elemet Method (FEM), has been implemented in a software tool named MAVICYS, Mechanical Analysis of VIscoelastic Composite CYlinderS. It takes into account geometry, stacking sequence, multistep manufacturing process, material thermo viscoelastic anisotropic behaviour, thermal expansion and chemical shrinkage of composite as well as heat transfer, cure kinetic and mechanical modelling of gelation.

Thermo viscoelastic behaviuor of the materials has been characterised by Dynamical Mechanical Analysis (DMA) tests. Convective thermal exchange coefficients within the autoclave chamber have been experimentally characterized. Embedded FBG sensors have been used for monitoring the strain inside cylinder during the whole multi-step manufacturing process. Fibre optic sensors revealed their effectiveness for composite applications since their dimensions are suitable for

embedding within the stacking sequence without altering the composite integrity [2,3,4]. In addition FBG sensors have been used to provide information on the degree of cure and the evolution of the process induced strains [5].

2 EFFECT OF THE PROCESS PARAMETERS ON RESIDUAL STRESSES

2.1 Evolution of material thermal properties during the cure of polymer

For modelling thermal phenomena in autoclave chamber, heat balance solved equation is:

$$c_p \rho \frac{\partial T}{\partial t} = k \frac{\partial^2 T}{\partial r^2} + k \frac{1}{r} \frac{\partial T}{\partial r} + \rho_r H_r (1 - v_f) \frac{\partial \chi}{\partial t} \tag{1}$$

where T is the temperature, r is radial coordinate, ρ and ρ_r the composite and resin density, k the radial conductivity, c_p the composite thermal capacity, H_r the heat reaction, v_f the volumetric fiber fraction and χ is the degree of cure. The kinetic of the chemical crosslinking reactions has been set according to the equation:

$$\frac{\partial}{\partial t}\chi = K_1 (1 - \chi)^{m_1} + K_2 (1 - \chi)^{m_2} \tag{2}$$

where the parameters K_1 and K_2 are calculated as [7],[8]:

$$\frac{1}{K_i} = \frac{1}{K_{Ti}(T)} + \frac{1}{K_{di}}, \qquad K_{Ti}(T) = A_i e^{-\frac{E_i}{RT}} \tag{3}$$

$$K_{di} = K_{di0} \exp\left(\frac{E}{R}\left(\frac{1}{T} - \frac{1}{T_g}\right)\right) \quad T < T_g, \qquad K_{di} = K_{di0} \exp\left(\frac{C_1 \left(T - T_g(\chi)\right)}{C_2 + T - T_g(\chi)}\right) \quad T > T_g \tag{4}$$

where T_g is the glass transition temperature given by the DiBenedetto equation [9],[11]:

$$T_g = \frac{(1 - \chi) T_{g0} + \lambda \chi T_{gi}}{(1 - \chi) + \lambda \chi} \tag{5}$$

with $= 0{,}69\ T_{g0} = 6°, T_{gi} = 115°$, while $m_1, m_2, k_{1d0}, k_{2d0}, A_1, A_2, E_1, E_2, C_1, C_2$ are parameters individuated through a fitting procedure to the experimental data achieved by Differential Scanning Calorimetry (DSC) tests on resin [10].

Table 1 reports the thermal parameters for the air, tool and composite. Finally, the internal and external to the cylinder heat exchange coefficients h_{int} and h_{ext} have been obtained through an experimental campaign aimed to the thermal characterization of the chamber.

2.2 Thermo-viscoelastic equation of the composite

In present analysis the thermo-mechanical properties have been characterized by experimental tests on the composite ply. The following stress and total strain components have been considered for the analysis:

$$\begin{aligned} \boldsymbol{\sigma} &= [\sigma_r \ \ \sigma_\theta \ \ \sigma_z \ \ \tau_{r\theta} \ \ \tau_{rz} \ \ \tau_{\theta z}]^T \qquad \boldsymbol{\varepsilon} = [\varepsilon_r \ \ \varepsilon_\theta \ \ \varepsilon_z \ \ \gamma_{r\theta} \ \ \gamma_{rz} \ \ \gamma_{\theta z}]^T \\ \boldsymbol{\sigma}' &= [\sigma_1 \ \ \sigma_2 \ \ \sigma_3 \ \ \tau_{12} \ \ \tau_{13} \ \ \tau_{23}]^T \qquad \boldsymbol{\varepsilon}' = [\varepsilon_1 \ \ \varepsilon_2 \ \ \varepsilon_3 \ \ \gamma_{12} \ \ \gamma_{13} \ \ \gamma_{23}]^T \end{aligned} \tag{6}$$

where the r, θ, z subscripts represents respectively the radial, angular and axial global cylindrical coordinate system, while 1,2,3 subscripts indicate the local ply axes, 1 for the local fibre axis, 2 and 3 respectively for transverse and the through thickness directions. The coordinate transformation are the rotation rules:

$$\boldsymbol{\sigma} = \boldsymbol{T}\boldsymbol{\sigma}' \qquad \boldsymbol{\varepsilon} = \boldsymbol{K}\,\boldsymbol{T}\boldsymbol{K}^{-1}\boldsymbol{\varepsilon}' \tag{7}$$

where $\boldsymbol{T}$ is the 6th order square rotation matrix depending by the ply wrapping angle φ, while $\boldsymbol{K}$ is the diagonal matrix transforming the engineering strain components in the tensorial ones. In the local ply reference system, the constitutive viscoelastic equation allows to express the stress components by the convolution integral on the full past strain history [13],[14],[16]:

$$\boldsymbol{\sigma}'(t) = \int_0^t \boldsymbol{Q}'\big(T_r, \chi_r, \xi(t) - \xi'(\tau)\big) \frac{\partial}{\partial \tau} [\boldsymbol{\varepsilon}'(\tau) - \boldsymbol{\varepsilon}'^{\,th}(\tau) - \boldsymbol{\varepsilon}'^{\,ch}(\tau)] d\tau \tag{8}$$

In eq. (8), t is the current time, τ the past time $\varepsilon'^{\,th}(\tau)$ and $\varepsilon'^{\,ch}(\tau)$ respectively the thermal expansion and the chemical shrinkage strains histories, T_r the reference temperature, χ_r the reference degree of cure, $\xi(t)$ and $\xi'(\tau)$ respectively the reduced current time and the reduced past time, defined by [13],[14],[15],[16]:

$$\boldsymbol{\xi}(t) = \int_0^t \frac{d\tau}{a_T\big(T(\tau), \chi(\tau)\big)} \qquad \boldsymbol{\xi}'(\tau) = \int_0^\tau \frac{d\tau}{a_T\big(T(\tau), \chi(\tau)\big)} \tag{9}$$

where a_T represents the horizontal shift factor at a temperature T and the degree of conversion χ. Finally Q' is the visco-elastic stiffness matrix in the local ply reference system at reference conditions. For an Unidirectional (UD) transversally isotropic layer, Q' is given by [13],[16]:

$$\boldsymbol{Q}'_{\boldsymbol{ref}}(t) = \begin{pmatrix} Q_{11}(t) & Q_{12}(t) & Q_{12}(t) & 0 & 0 & 0 \\ Q_{12}(t) & Q_{22}(t) & Q_{23}(t) & 0 & 0 & 0 \\ Q_{12}(t) & Q_{23}(t) & Q_{22}(t) & 0 & 0 & 0 \\ 0 & 0 & 0 & Q_{44}(t) & 0 & 0 \\ 0 & 0 & 0 & 0 & Q_{44}(t) & 0 \\ 0 & 0 & 0 & 0 & 0 & [Q_{11}(t) - Q_{12}(t)]/2 \end{pmatrix} \tag{10}$$

The Q_{ij} components represent the anisotropic relaxation modules of the material. For each Q_{ij}, the rheological model the Generalized Maxwell element has been considered composed by 10 parallel Maxwell viscoelastic elements with an extra spring. According to this choice, the relaxation modules $Q_{ij}(t)$ can be expressed by the exponential Prony series expansion [12],[13]:

$$Q_{ij}\big(T_r, \chi_r, \xi(t) - \xi'(\tau)\big) = E_{0,ij} + \sum_{k=1}^{N} E_{k,ij} e^{\left(-\frac{\xi(t) - \xi\prime(\tau)}{\tau_{k,ij}}\right)} \tag{11}$$

where $E_{k,ij}$ and $\tau_{k,ij}$ are respectively the temperature and the cure dependent modules and relaxation times. Experimental investigations on the UD employed tapes have been carried out for determination of the $E_{k,ij}$ and $\tau_{k,ij}$ in eq. (11). Experimental techniques were based on Dynamical Mechanical Analysis (DMA) tests, performed on the plies at different temperatures and frequencies. The effect of the temperature and of the degree of cure was considered by applying the time-temperature superposition (TTS) principle [12],[13], assuming simple thermo-rheological behaviour of the material. The experimental data $Q_{ij\,storg}(\omega, T)$ in the frequency domain were shifted on a single Master-curve $Q^M_{ij\,storg}\big(\omega, T_{ref}\big)$, relative to the reference temperature T_{ref}. Shift factors $a_T(T, \chi)$ in eq. (9) were modelled according to the Williams-Landel-Ferry (WLF) equation:

$$log_{10}(a_T) = -\frac{c_1\big(T - T_{ref}\big)}{c_2 + T - T_{ref}} \tag{12}$$

where c_1 e c_2 were found through fitting procedure on the shift factors values employed to build the master curve in the frequency domain. The effect of the degree of cure was taken into account by choosing the T_{ref} as the glass transition temperature T_g, i.e. the temperature at which experimental DMA tests were performed:

$$T_{ref} = T_g(\chi) \tag{13}$$

The glass transition temperature on the resin T_g has been measured by Differential Scanning Calorimetry (DSC), and expressed through the Di Benedetto eq. (5). Finally, the thermal and chemical strains $\boldsymbol{\varepsilon}'^{\,th}$ and $\boldsymbol{\varepsilon}'^{\,ch}$ in eq.(8) have been calculated as:

$$\boldsymbol{\varepsilon}'^{th}(\tau) = \int_{T(\tau_r)}^{T(\tau)} \boldsymbol{\alpha}(T,\chi)dT \qquad \boldsymbol{\varepsilon}'^{ch}(\tau) = \int_{\chi(\tau_r)}^{\chi(\tau)} \boldsymbol{\beta}(T,\chi)d\chi \tag{14}$$

where $\boldsymbol{\alpha}(T,\chi)\ e\ \boldsymbol{\beta}(T,\chi)$ are respectively the thermal and chemical coefficients vectors as function of temperature and degree of cure, determined by experimental tests on the unidirectional carbon fiber layer. Dependence by temperature of thermal expansion coefficients were calculated assuming a sigmoidal behavior expressed by:

$$\alpha_i(T,\chi) = \alpha_i^{Glassy} + \left(\alpha_i^{Rubbery} - \alpha_i^{Glassy}\right)\left(1 + e^{-\frac{T-T_g}{A}}\right)^{-1} \qquad A = 2.5°C \tag{15}$$

in which T_g is the glass transition temperature, α_i^{Glassy} and $\alpha_i^{Rubbery}$ were supplied by the experimental characterization and the A parameter defines the amplitude of the transition range.

2.3 Multistep fabrication

In present work MultiStep (MS) manufacturing process is analyzed. In MS process, final cylinder thickness is obtained by multiple stages of plies wrapping and curing cycles in the autoclave chamber. At the beginning of each curing stage, free stress and strain condition in last joined plies was always assumed.

2.4 Numerical Analysis

For axial symmetric problems all the derivatives with respect to the angular coordinate ϑ vanish. Equilibrium equations become:

$$\frac{\partial \sigma_r}{\partial r} + \frac{\partial \tau_{rz}}{\partial z} + \frac{\sigma_r - \sigma_\theta}{r} = 0 \tag{16}$$

$$\frac{\partial \tau_{r\theta}}{\partial r} + \frac{\partial \tau_{\theta z}}{\partial z} + 2\frac{\tau_{r\theta}}{r} = 0 \tag{17}$$

$$\frac{\partial \tau_{rz}}{\partial r} + \frac{\partial \sigma_z}{\partial z} + \frac{\tau_{rz}}{r} = 0 \tag{18}$$

Boundary conditions require that on the external laminate surface the radial stress must be the opposite of autoclave chamber environmental pressure $p(t)$ and the tangential stresses must be nil:

$$\sigma_r(R_n^e, t) = -p(t), \qquad \tau_{r\theta}(R_n^e, t) = 0, \qquad \tau_{rz}(R_n^e, t) = 0 \tag{19}$$

where R_n^e is the external radius of the last n-th layer wrapped. On the other hand, the boundary conditions on the internal laminate surface require modeling of structural and thermal behavior of tool, in order to take into thermo-mechanical interaction with the composite plies during cure:

$$\boldsymbol{\varepsilon}_{tool} = \boldsymbol{\alpha}_{tool}(T - T_0) \tag{20}$$

where $\boldsymbol{\alpha}_{tool}$ is the CTE tool, while T_0 the initial temperature. Tool-composite tangential interaction was modeled by considering an extra resin thin layer between tool and composite.

According to FEM procedure, spatial domain in r-z section was divided in multiple quadrangular axial-symmetric elements, having displacement fields u_r, u_θ, u_z approximated by linear polynomial expressions (shape functions) in the r, θ, z coordinates. Stiffness matrices for axy-symmetric quadrangular elements were directly calculated from virtual work principle in the viscoelastic case. Equilibrium equation in the global cylindrical coordinate for i-th element at current time t lead to:

$$\int_0^t \int_V (\boldsymbol{DN}_i)^T \boldsymbol{T}_{\varphi_i} \boldsymbol{Q}_i'\left(T_r, \chi_r, \xi(t) - \xi'(\tau)\right) \frac{\partial}{\partial \tau}\left[\boldsymbol{T}_{\boldsymbol{\varepsilon}}^{-1} \boldsymbol{DN}_i \boldsymbol{u}^i(\tau) - \boldsymbol{\varepsilon}_i'^{th}(\tau) - \boldsymbol{\varepsilon}_i'^{ch}(\tau)\right] dV\, d\tau = \boldsymbol{F}_i \tag{21}$$

where $\boldsymbol{F}_i$ is the i-th element nodal force vector, $\boldsymbol{N}_i$ is the shape function matrix, $\boldsymbol{u}^i$ the nodal displacements, $\boldsymbol{D}$ the differential strain operator in cylindrical coordinates:

$$\boldsymbol{D^T} = \begin{pmatrix} \frac{\partial}{\partial r} & \frac{1}{r} & 0 & 0 & \frac{\partial}{\partial z} & 0 \\ 0 & 0 & 0 & -\frac{1}{r}+\frac{\partial}{\partial r} & 0 & \frac{\partial}{\partial z} \\ 0 & 0 & \frac{\partial}{\partial z} & 0 & \frac{\partial}{\partial r} & 0 \end{pmatrix} \tag{22}$$

and

$$\boldsymbol{T_\varepsilon}^{-1} = \boldsymbol{K}\,\boldsymbol{T}^{-1}\,\boldsymbol{K}^{-1} \tag{23}$$

Once achieved the global stiffness matrix through assembling, the algebraic solving system was solved for each time step, to get the last unknown displacement variation $\Delta\boldsymbol{u}_n^{\boldsymbol{F}}$ of all unconstrained nodes:

$$\Delta\boldsymbol{u}_n^{\boldsymbol{F}} = \left(\boldsymbol{K}_{\boldsymbol{n}}^{\boldsymbol{F}}\right)^{-1}\left[\boldsymbol{F}^F + \boldsymbol{K}_n^{\boldsymbol{F}\,th+ch}\Delta{\boldsymbol{\varepsilon}'}_n^{\boldsymbol{F}\,th+ch} - \sum_{s=1}^{n-1}\left(\boldsymbol{K}_s^{\boldsymbol{F}}\Delta\boldsymbol{u}_s^{\boldsymbol{F}} - \boldsymbol{K}_s^{\boldsymbol{F}\,th+ch}\Delta{\boldsymbol{\varepsilon}'}_s^{\boldsymbol{F}\,th+ch}\right)\right] \tag{24}$$

where $\boldsymbol{K}$ symbol indicates the generic stiffness matrix, F superscript the corresponding sub-matrices relative to the free nodes only, s is the s-th temporal step, n the last time step. After the determination of the nodal displacement $\boldsymbol{u}_n$, the stress and the strain for i-th element were calculated as:

$$\boldsymbol{\varepsilon_i}(t_n) = \boldsymbol{D}\boldsymbol{N}_i\boldsymbol{u}_n^i \tag{25}$$

$$\boldsymbol{\sigma}_i(t_n) = \boldsymbol{T}_{\varphi_i}\sum_{s=1}^{n}\boldsymbol{Q}_i{}'\left(T_r, \chi_r, \xi(t_n) - \xi'(t_s)\right)\left(\boldsymbol{T}_{\boldsymbol{\varepsilon}\,\varphi_i}^{-1}\boldsymbol{D}\boldsymbol{N}_i\Delta\boldsymbol{u}_s^i - \Delta{\boldsymbol{\varepsilon}_i}'_s{}^{th+ch}\right) \tag{26}$$

As long as the degree of conversion in a generic position is lower than the conversion at gel point, the reference strain of zero stress condition for fully relaxed material is considered to take into account gelation process.

Final evaluation of failure risk is then carried out employing one of failure criterion available from literature. For example, by neglecting interaction terms in the form $\sigma_i\sigma_j\ \ i \neq j$, Tsai-Wu failure criterion states that failure occurs when [17]:

$$\frac{X_t+X_c}{X_tX_c}\sigma_1 + \frac{Y_t+Y_c}{Y_tY_c}(\sigma_2+\sigma_3) - \frac{\sigma_1^2}{X_tX_c} - \frac{\sigma_2^2+\sigma_3^2}{Y_tY_c} + \frac{\tau_{12}^2}{T_{12}^2} + \frac{\tau_{13}^2}{T_{13}^2} + \frac{\tau_{23}^2}{T_{23}^2} \geq 1 \tag{27}$$

where X_t e X_c are the tensile and compression failure stresses in the fiber direction, Y_t and Y_c are the tensile and compression failure stresses in the transverse to the fiber direction, while $T_{12}\ T_{13}\ T_{23}$ are the shear failure stresses.

Property	Symbol	Value	Property	Symbol	Value
Air Thermal Conductibility	k_{air}	0,024 W K^{-1} m^{-1}	Tool (Steel) Thermal Conductibility	k_{steel}	50 W K^{-1} m^{-1}
Air Density	ρ_{air}	1,29 Kg m^{-3}	Tool (Steel) Density	ρ_{steel}	7800 Kg m^{-3}
Air Heat Capacity	C_{air}	1000 J Kg^{-1} K^{-1}	Tool (Steel) Heat Capacity	C_{steel}	486 J Kg^{-1} K^{-1}
Composite Thermal Conductibility	k_c	0,8 W K^{-1} m^{-1}	De ext. diameter		105 mm
Composite Density	ρ_c	1630 Kg m^{-3}	Di inner diameter		89 mm
Composite Heat Capacity	C_c	1053 Kg m^{-3}	Tool Material		Iron Fe 52
Section		open	0° Layer thickness		0.444 mm
Staking sequence		$[0_2/+45/-45/0_2]_8$	45° Layer thickness		0.174 mm

Table 1 – Geometrical and Physical parameters

3 EXPERIMENTALS

3.1 Radial and axial strain measurement

A FBG is a periodic and permanent modification of the core refractive index along the optical fibre axis. A FBG is defined by the grating length, i.e. the gauge length where the index modulation have been realised; the periodicity (Λ) and the amplitude (δ_n). The perturbation in the fibre core

induces light coupling in two propagating modes inside the core, the mode coupling occurs for some wavelength around the Bragg wavelength defined by [20]:

$$\lambda_{Bragg} = 2\, n_{eff}\, \Lambda \tag{28}$$

Where n_{eff} is the effective refractive index of the core at Bragg wavelength. The effective refractive index of the core and spatial periodicity of the grating are both affected by the changes in temperature and strain.

$$\frac{d\lambda}{\lambda} = (1 - P_e)\, d\varepsilon + (\alpha_{glass} + \zeta)\, dT \tag{29}$$

Where P_e is the elasto-optic coefficient (0.22 adimensional) while the thermal sensitivity is about 6.67 10^{-6} /°C for optical fibre whose core is silicon dioxide.

3.2 Manufacturing of the component

A composite cylinder whose stacking sequence is $[0/0/+45/-45/-45/45/0/0]_8$ was manufactured. Table 1 reports the geometrical dimensions and the material of the tool. According to table 1 the 45° layer are 0.174 mm thick, while 0° layers are 0.444 thick.

The manufacturing process is divided in four separated steps, at each step three FBG array have been integrated within the composite: two bare arrays have been embedded directly in the composite material while a third array is considered for temperature compensation during the test.

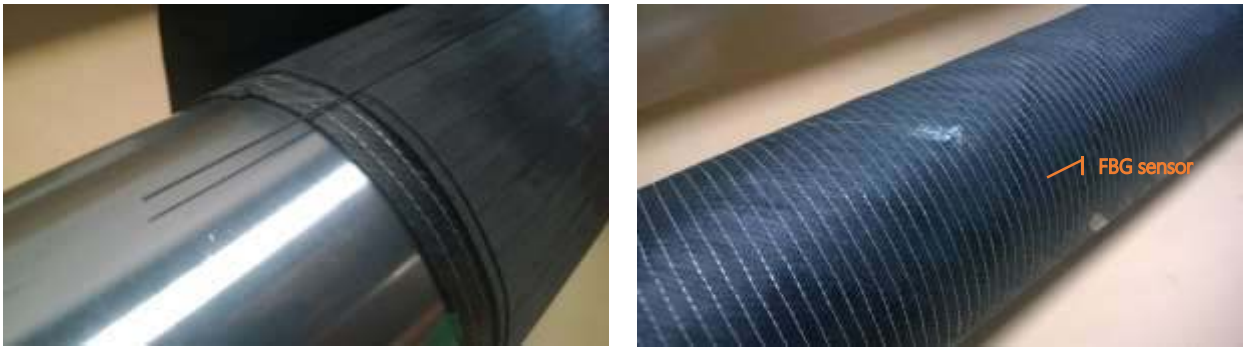

a) b)

Figure 1 - Composite tape and FBG array positioning.

Autoclave air temperature during each thermal cycle is set to ramp up from 20°C (room temperature) to 120°C in 1h 30 min, with a single dwell. The dwell has 5h 30 min of lifespan. Subsequently the temperature is cooled down from 120° to the room temperature (20 °C) in 2h 20 min. The pressure in the autoclave chamber is set to follow the temperature-time profile from 1bar. During dwell the nominal pressure is kept at 4bar (0.4 MPa).

Figure 1 reports the installation of the FBG arrays on the composite cylinder: a previously cut composite layer is first wrapped on the tool (first step) or on the external surface (further steps) of the composites. Finally the plies have been wrapped on the tool with a pneumatic press.

Each array contain two sensors spaced 30 centimetres, sensors were installed 30 centimetres far from cylinder edges to reduce boundary effects. The installation of free strain sensor is divided in two parts, during wrapping stage a hollow carbon pipe is embedded in the composite cylinder then before bagging stage TS array is inserted Figure 1-a). At each manufacturing step a couple of sensor is added, moreover a temperature sensor is provided for temperature compensation purpose. For each manufacturing step an FBG array has been arranged along 45° fibres and another has been arranged along cylinder axis fibres Figure 1-b).

When all the required tapes have been wrapped on the tool, the cylinder is enveloped by nylon

strips. Below the bag, a fabric is applied in order to make easier the adhesion to further lamination steps.

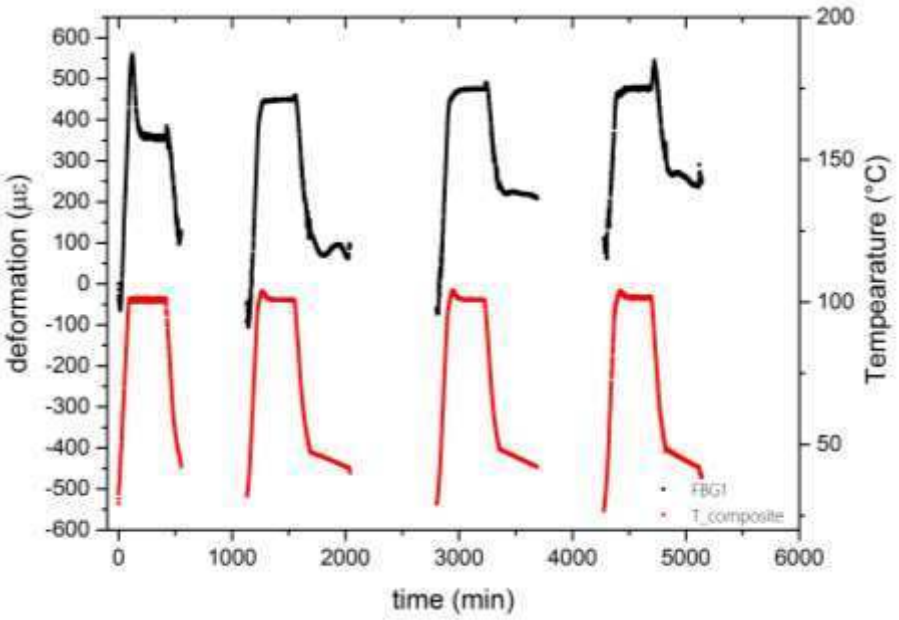

Figure 2 - Deformation experienced during manufacturing steps.

Figure 2 reports the thermo-mechanical strain evolution experienced by the first FBG array (hereinafter-named FBG1) during all the manufacturing steps, on the right axis of the picture the composite temperature profile (red line) is drawn. FBG1 array have been along 45 degrees direction (Figure 1-b). In the first manufacturing stage (first cure step, heating-dwell-cooling) an overshoot in the deformation is clearly visible related to the cure of the polymer matrix while in further stages it disappears, since the material is fully cured.

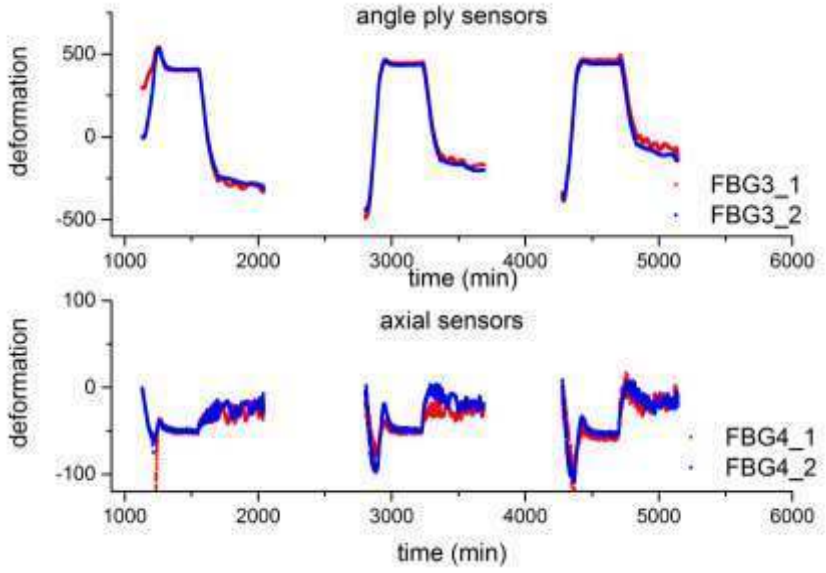

Figure 3 - Strain history for sensors installed over the first lamination step

Each arrays (including two sensors) have been installed at constant radius and different position along cylinder axis. Figure 3 show the deformation experienced from sensors installed upon the first lamination (second manufacturing step). Experimental data confirm the symmetric behaviour of the system. Deformations experienced from sensors on the same array (namely at constant radius) overlapping each other with very good approximation. In the last lamination step the load applied by the external additional material induces a the deformation on inner radii sensors sensor leading to horn-like strain profiles.

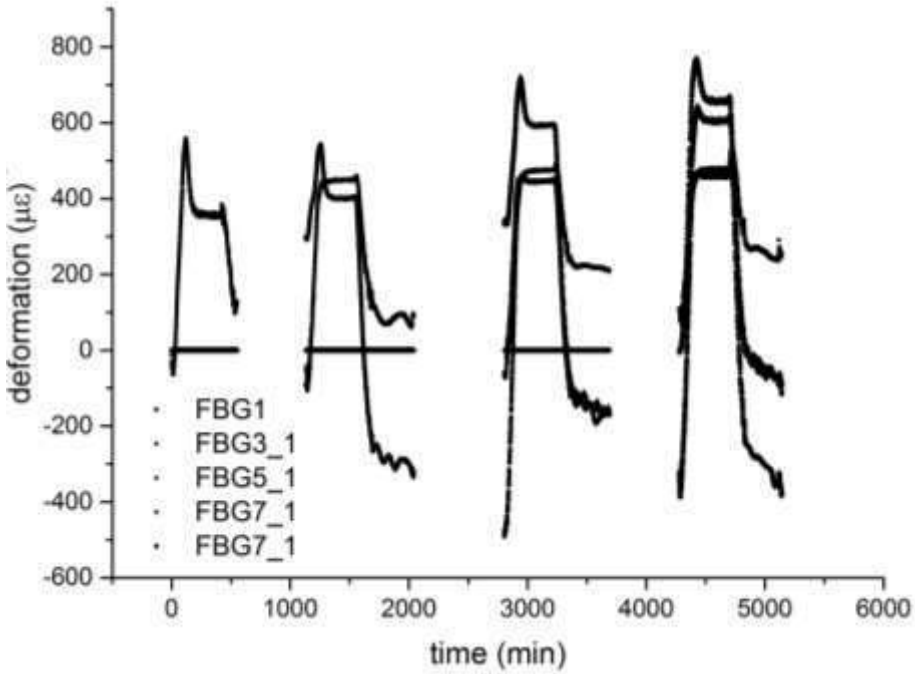

Figure 4 – Deformation experienced on sensors over all the process

Figure 4 reports in addition the deformation histories experienced by the sensors installed during the further manufacturing stages. In the pictures, only data relative to the sensors oriented on the 45° direction have been reported; sensors aligned as the cylinder axis reproduced the same behaviour of array FBG4 (Figure 3). Those sensors experienced a slight negative peak during the heating with an average zero deformation status. Picture shows that the longitudinal strains changes during the cure cycle are almost negligible.

4 NUMERICAL RESULTS

The comparison between the numerical results for the first 3 manufacturing steps and the experimental measures (FBGs are everywhere aligned with local fiber direction of UDs plies) is presented in the Figure 5. At same colour line corresponds the same position. Numerical predictions showed excellent agreement with experimental data, all over the manufacturing process. When the composite has a rubbery behaviour, and due to higher mechanical stiffness of the steel-made tool, the hoop thermal expansion of the tool is transmitted to the composite, while the axial thermal strain (0° FBGs) isn't.

Experimental FBG measures for 45° layer show a marked strain overshoot before the stabilization on the dwell strain level. The shrinkage of the resin during the cure may only partially explain this phenomenon. Alternative hypothesis can explain this effect by considering the pressure in the autoclave environment. At the onset of curing, indeed, the resin presents a very low modulus (rubbery stage) and the action of the pressure is consistent with a hoop compression of the composite laminate. When resin completes cure, the transversal ply modulus increases, and the FBG strain level stabilizes. Numerical predictions shows that gel point is reached shortly after dwell onset.

Relatively to the evaluation of the risk of failure, Figure 6 shows the calculated Tsai-Wu coefficient for the examined stacking sequence. On left side of the figure, the Tsai-Wu coefficient is shown as a function of the radial positions at different times, marked by different colours (from blue line, relative to initial simulation time to dark red line, for final simulation time); the gray dashed lines indicates the interface between the plies wrapped at different steps; the local ply angle can be read on the right hand scale.

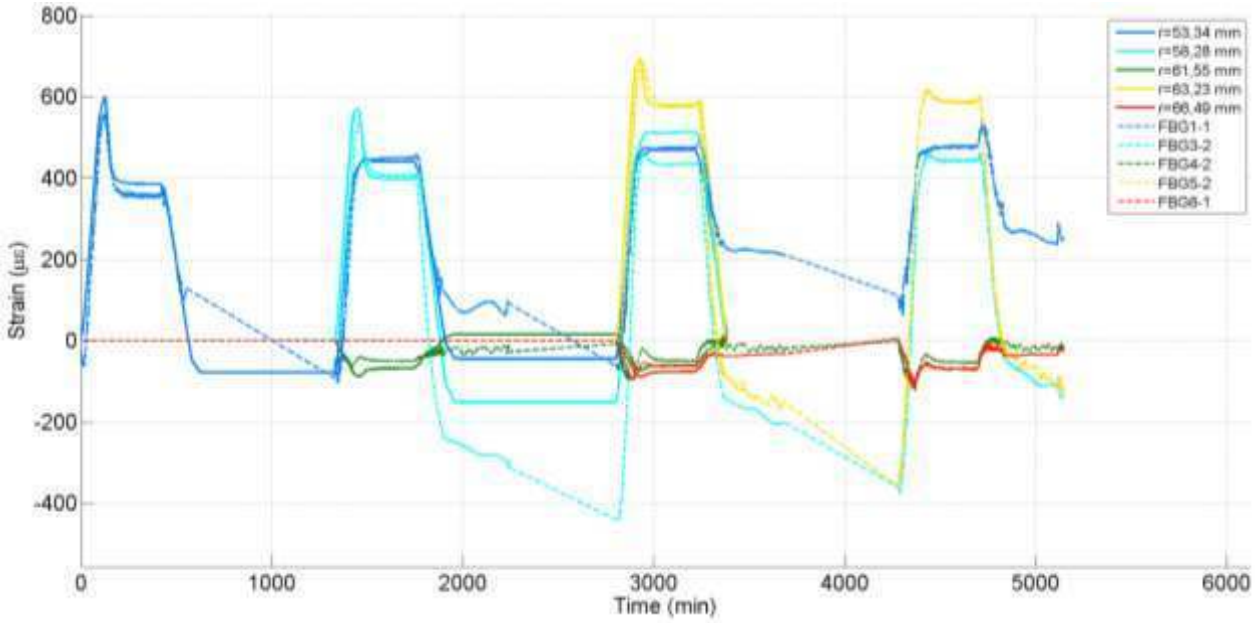

Figure 5: Comparison between experimental data (dashed lines) and numerical results (solid lines, first 3 steps)

The evolution of the Tsai Wu coefficient (dark blue line for most internal position, dark red line for the most external) is shown on the right. The figure points out that risk of failure during manufacturing for this configuration is quite high, up to about 0.68 during 2nd step at external 45° layer positions.

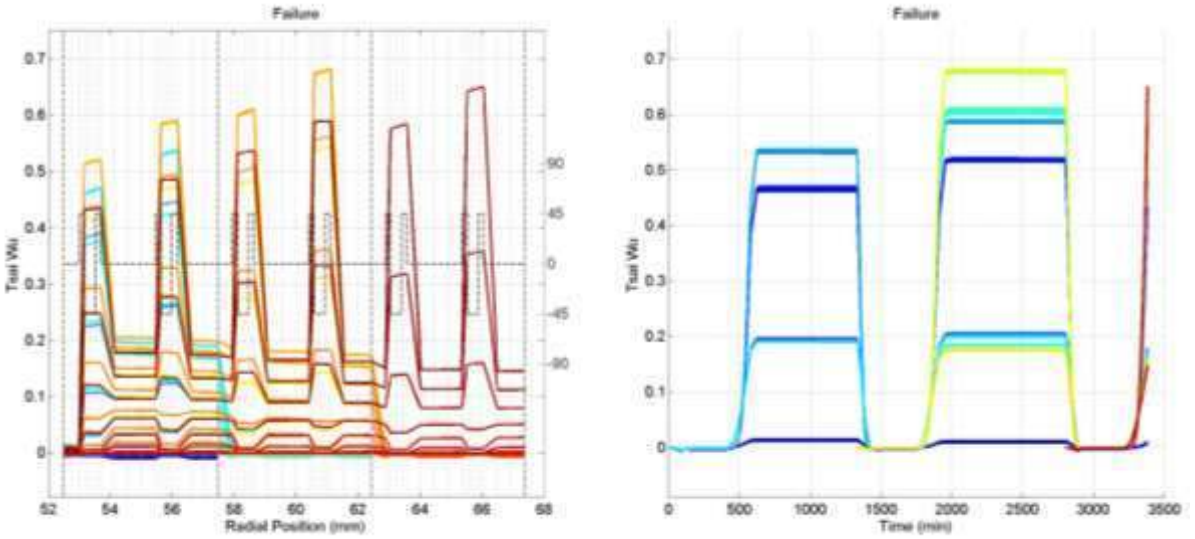

Figure 6: Faliure Tsai-Wu coefficient achieved from numerical simulation of the manufacturing process

5 CONCLUSIONS

The autoclave process is the main and most largely diffuse technology for high quality polymer composite manufacturing. In the case of thick composite parts, the process often produces distortion and residual stresses. In this work a thermo viscoelastic anisotropic mechanical FEM model is developed for the evaluation of the risk of failure during the fabrication of a thick composite cylinder. In order to validate the numerical model, FBG optical sensors have been embedded within the composite plies to measure the strain during the production process. Numerical predictions showed excellent agreement with the experimental data. In addition, numerical results predict that the risk of failure is not completely negligible, in accordance with some case of failures really occurred during the manufacturing of thick composite cylinders.

REFERENCES

[1] Fonseca G.E., Dubè M.A., Penlidis A., A Critical Overview of sensors for Monitoring Polymerizations. Macromolecular Reaction Engineering, Vol 3, pp327-373, 2009.

[2] Konstantopoulos S., Fauster E., Schledjewski R., Monitoring the production of FRP composites: A review of in-line sensing methods. Express Polymer Letters, Vol. 8, p823-840, 2014.

[3] V. Antonucci, M. Giordano, A. Cusano, J. Nasser, L. Nicolais, Real time monitoring of cure and gelification of a thermoset matrix, Composites Science and Technology, Vol. 66, 2008.

[4] Fernando G.F., Fibre optic sensor systems for monitoring composite structures. Reinforced Plastics, Vol. 49, pp. 41-50, 2005.

[5] D. Karalekas, J. Cugnoni, J. Botsis, Monitoring of process induced strains in a single fibre composite using FBG sensor: A methodological study, Composites Part A: Applied Science and Manufacturing,

[6] Antonucci V., Giordano M., Imparato S.I., Nicolais L., Autoclave Manufacturing of Thick Composites, Polymer Composites, Vol. 23, Issue 5, 2002.

[7] E. Rabinowitch, in Transaction Faraday Society, 33, 1225, (1937)

[8] C. W. Wise, W. D. Cook and A.A. Goodwin, in Polymer, 38, 3251, (1997)

[9] Hale A., Macosko C.W.,Bair E.H.,Glass transition temperature as a function of conversion in thermosetting polymers, Macromolecules, Vol 24 (9),pp. 2610-2621, 1991.

[10] Luo Z., Wei L., Li W., Liu F., Zhao T., in Journal of Applied Polymer Science, Vol 109, pp. 1097-4628, 2006.

[11] Di Benedetto A. T., Prediction of the glass transition temperature of polymers: A model based on the principle of corresponding states, Journal of Polymer Science Part B: Polymer Physics, Vol 25, pp. 1949-1969,1987.

[12] J. D. Ferry, in *"Viscoelastic Properties of Polymer"*, John Wiley & Sons, Inc, (1976)

[13] S.R. White and Y.K. Kim, Process-Induced Residual-Stress Analysis Of As4 3501-6 Composite-Material/ Mechanics of Composite Materials and Structures, 5, 153, (1998)

[14] K.S. Kim and H.T. Hahn - Residual stress development during processing of graphite/epoxy composites - in Composite Science and Technology, 36, 121, (1989)

[15] Kim Y.K., White S.R., Stress relaxation behaviour of 3501-6 epoxy resin during cure, Polymer Engineering & Science, Vol.36, pp. 2852-2862, 1996

[16] H.Y. Hwang, Y.K. Kim, C. Kim, Y.D. Kwon, W.Choi, Thermo-Viscoelastic Residual Stress Analysis of Metal Liner-Inserted Composite Cylinders (2003)

[17] Tsai SW, Wu EM. A general theory of strength for anisotropic materials. J Compos Mater 1971;5(1):58–80.

[18] Maffezzoli, A Grieco, A., Optimization of Parts Placement in Autoclave Processing of Composites Journal of Applied Composite Materials, Vol. 20 (3), 2012.

[19] A. Martone, M. Esposito, V. Antonucci, M. Zarrelli, M. Giordano, In-Autoclave Residual Stress Progression during Multiple Step fabrication of Composite Cylinders, ICCST/10

[20] R. Rajinikumar, M. Süßer, K.G. Narayankhedkar, G. Krieg , M.D. Atrey in Cryogenics 2009

AKNOWLEDGEMENT

This activity has been performed within the seventh framework program, grant "SCYPRI-Smart Cylinders for Flexographic Printing Industry". The Authors would like to thanks Reglass staff who actively contribute to in-autoclave experimentations.